Bioelectrochemistry 128 (2019) 274–282

Contents lists available at ScienceDirect

Bioelectrochemistry

journal homepage: www.elsevier.com/locate/bioelechem

Fabrication of hexahedral Au-Pd/graphene nanocomposites biosensor and its application in cancer cell H_2O_2 detection

Wenhao Dong [a], Yipeng Ren [b], Zhixue Bai [c], Yi Yang [d], Qiang Chen [a,*]

[a] The Key Laboratory of Bioactive Materials, Ministry of Education, College of Life Science, Nankai University, Weijin Road No. 94, Tianjin 300071, PR China
[b] Institution of Entomology, College of Life Science, Nankai University, Tianjin 300071, PR China
[c] The RNA Institute, University at Albany-SUNY, Albany, NY, USA
[d] Tianjin Medical University Cancer Institute and Hospital, National Clinical Research Center for Cancer, Key Laboratory of Cancer Prevention and Therapy, Tianjin, Key Laboratory of Breast Cancer Prevention and Therapy, Tianjin Medical University, Ministry of Education, Huan-Hu-Xi Road, Tianjin 300060, PR China

ARTICLE INFO

Article history:
Received 14 February 2019
Received in revised form 24 April 2019
Accepted 24 April 2019
Available online 26 April 2019

Keywords:
Electrochemical biosensors
Three-dimension nanostructure
Hydrogen peroxide
Cancer cells
Reactive oxygen species

ABSTRACT

Currently, real time monitoring of chemical substances *in vivo* and *in vitro* has gained enormous attraction, and many researches reports have been focused on the design and construction of high-performance biosensor devices. In this work, a high-performance sensor was constructed by taking advantage of the excellent electrochemical activity and high-index facets of Au-Pd nanocubes and the large surface of rGO. Glassy carbon electrodes (GCEs) were modified by both Au-Pd nanocubes and rGO nanocomposites *via* physical adsorption. Transmission electron microscopy (TEM) and X-ray diffraction (XRD) were utilized to characterize and identify this unique nanostructure. These three-dimensional nanocomposites possess a high electroactive surface area and an excellent electrical conductivity, which resulted in favorable electroreduction activity toward H_2O_2 with a lower detection limit of 4 nM, a wide linear range from 0.005 μM to 3.5 mM and a rapid response time. Furthermore, the proposed sensor exhibited desirable performance in the detection of endogenous H_2O_2 in human serum samples and real-time monitoring of H_2O_2 released from living breast cancer cell lines. In summary, this work not only provides a potential method to construct a physiological and pathological H_2O_2 biosensor but also makes a valuable contribution to the early diagnosis of different cancers.

1. Introduction

Breast cancer has become a major and unsolved problem in women's healthcare all over the world. With >255,180 new breast cancer cases occurring in the United States each year, efforts to enhance early diagnosis and therapy resonate intensely both with sufferers and clinicians alike [1,2]. In addition, survival statistics vary greatly by stage at diagnosis; so, the corresponding therapy at an early stage is beneficial for improving the survival rates of breast cancer. Currently, typical techniques for the early diagnosis include mammography, biopsy, magnetic resonance imaging (MRI), ultrasound, thermography and endoscope, which lack the sensitivity for the detection of a cancer until it has metastasized to another organ [3–6]. Currently, many investigators are looking at ways of utilizing biosensors for cancer diagnosis with the attributes of high sensitivity for effective detection of cancer biomarkers at an early stage [7–9].

Emerging evidence suggests that many types of cancer cells have excessive levels of reactive oxygen species (ROS) compared with their normal counterparts [10,11]. Hydrogen peroxide (H_2O_2) is one of the most important ROS and is associated with various pathological and physiological processes. Furthermore, excessive amounts of H_2O_2 can cause damage to proteins, lipids and DNA within cells to cause various diseases, such as cancer, Alzheimer's, heart attacks and Parkinson's disease [12,13]. Moreover, due to cancer cells generating excessive amounts of H_2O_2 compared to normal cells, H_2O_2 can be employed as a biomarker for evaluating the oxidative stress capability differences in diverse cells and the detection of cancer cells [14]. Therefore, the effective and accurate detection of H_2O_2 is essential to monitor its concentration in living cells and understand the relevant biological processes. Currently, the electrochemical analysis distinguishes itself due to its remarkable properties, such as high sensitivity, simplicity, low cost and rapidness, and has been used to detect H_2O_2 in living cells [5]. The electrochemical detection of H_2O_2 is divided into non-enzymatic and enzymatic sensors, but the typical enzymatic sensors are impractical for commercial application because of its high cost, low durability and high sensitivity to external conditions [15,16]. Therefore, much efforts has been devoted to developing the nano-enzymatic sensors variously constructed by noble metal nanoparticles, nonprecious mental nanoparticles, hydrogels and redox conducting polymers [17]. Up to now, only nano-enzymatic sensors fabricated using noble metal nanoparticles have shown good performance in the detection of H_2O_2 released

* Corresponding author.
E-mail address: qiangchen@nankai.edu.cn (Q. Chen).

https://doi.org/10.1016/j.bioelechem.2019.04.018
1567-5394/

from living cells [18,19]. Thus, an improved sensor based on noble metal nanoparticles warrants development.

Synergistic effects, in which two or more nanoparticles were combined exhibited much higher activity than the additive effect of two particles used individually [20,21]. Compared with sensors based on individual noble metal nanoparticles, bimetallic noble metal nanoparticles present excellent catalytic performance in electrochemistry due to synergistic effects [22–24]. However, there are many limitations that restrict their further applications in H_2O_2 sensors, such as undesirable high sensitivity and detection limits reached at the nM level [25]. In addition, the control of bimetallic nanocomposites in both size and shape can greatly improve their electrocatalytic activity, which results from their high-index facets [26,27]. Fundamental researches has shown that metal nanoparticles with high-index planes usually present much higher catalytic activity than those with common stable planes, serving as active sites for breaking chemical bonds with high density atomic steps, kinks and ledges [28,29]. Based on this, fabrication efforts have been devoted to synthesizing bimetallic compounds with different shapes, including cubic, tetrahexahedral and cuboctahedral. Kakati et al. [30] reported a technique for sensing urea based on hollow sodium nickel fluoride nanocube-deposited MWCNT, and the device showed good accuracy and electrocatalytic activity. Graphene, a two-dimensional carbon nanostructure, is often chosen as the supporting material, due to its specific surface area and higher electronic conductivity [31–33]. Previous research has suggested that dispersing noble metal nanocomposites in a scaffold such as graphene can greatly enhance the stability and catalytic activity of a sensor [34,35]. For example, Sun et al. [25] synthesized graphene/PtPd nanoplates for the electrochemical detection of H_2O_2 released from Raw 264.7 cells, and the sensor showed a high sensitivity and low detection limit for the reduction of H_2O_2.

The aim of this study was not only a novel bimetallic nanocomposite for a high sensitivity H_2O_2 sensor but also the monitoring of H_2O_2 release from breast cancer cells to enable cancer diagnosis. In this paper, we developed a sensor fabricated by assembling Au-Pd nanocube nanocomposites on the surface of reduced graphene oxide (rGO), the prepared nanocomposites were modified on a glassy carbon electrode (GCE) by physical adsorption. Subsequently, based on the specific nanostructure of the nanoalloy, the electrochemical signal was greatly enhanced, and the resulting sensor utilized for selective and sensitive detection of H_2O_2 in human serum to monitor H_2O_2 released from cultured breast cancer cell lines (MCF-7, MDA-MB-231 and T47D). This study is of value for further the investigation of early cancer diagnosis and drug discovery.

2. Experimental section

2.1. Reagents and materials

Palladium chloride ($PdCl_2$), hydrogen tetrachloroaurate trihydrate ($HAuCl_4{\bullet}3H_2O$), cetyltrimethylammonium bromide, cetyltrimethylammonium chloride (CTAC), cetyltrimethylammonium bromide (CTAB), ascorbic acid (AA), poly (diallyldimethylammonium) (PDDA) were all purchased from Sigma-Aldrich Inc. (St. Louis, MO, USA). Hydrochloric acid (HCl), potassium bromide (KBr), potassium iodide (KI) were obtained from Tianjin Chemical Regent Co., Ltd. (Tianjin, China). RPMI 1640 medium and fetal bovine serum were purchased from Gibco (Gaithersburg, MD, USA). rGO was synthesized on the basis of our previous report [36]. All regents were used without further purification, and ultrapure deionized (DI) water was used throughout all experiments.

2.2. Apparatus

Scanning electron microscopy (SEM, JSM-7500F, JEOL, Japan) and Transmission electron microscopy (TEM, Tecnai G2 F20, FEI, USA) were used to characterize the morphology of the nanostructure and the relevant composition. X-ray diffraction (XRD) patterns were recorded on a Rigaku D/max 2550 Powder X-ray diffractometer (Rigaku, Japan). Cyclic voltammetry (CV) and Chronoamperometry (*i-t*) were performed with a 283 potentiostat/galvanostat electrochemical analyzer (EG & GPARC, Japan) using a typical three-electrode system. The reference electrode was Ag/AgCl electrode (saturated KCl), the counter electrode was a platinum wire, and the working electrode was a bare or modified glassy carbon electrode (GCE). All the electrochemical tests were measured in a N_2-saturated phosphate buffer solution (0.1 M, pH 7.4) under room temperature.

2.3. Synthesis of Au-Pd nanocubes and a modified electrode

Au-Pd nanocubes were prepared as follows: first, 0.048 g of CTAC was dissolved in 8.65 mL of ultrapure deionized water in a flask, and the flasks were then kept in a water bath set at 31 °C. The H_2PdCl solution (0.75 mL, 10 mM) and as-prepared Au core solution (0.3 mL) were added, the reaction mixture was purged with high-purity nitrogen gas for 30 min and the ascorbic acid solution (0.3 mL, 0.1 M) was added above the mixture. The resultant mixture was placed undisturbed for 30 min, and then washed three times with ultrapure deionized water. Before the electrochemical measurement, the GCE was successively polished with aluminium oxide power (0.3 and 0.5 μm) to obtain a specular surface and sonicated with ultrapure deionized water and anhydrous ethanol for 5 min. The cleaned GCE was dried under high-purity nitrogen gas. Subsequently, to fabricate Au-Pd/rGO-modified electrodes, 6 μL of the Au-Pd nanocube and rGO dispersion (1,1) was cautiously cast onto the surface of a newly polished GCE and dried naturally. As a control, 6 μL of Au-Pd nanocube solution and 6 μL of rGO suspension were separately dropped on the same GCE. The obtained electrodes are denoted as Au-Pd/GCE and rGO/GCE.

2.4. Electrochemical detection of H_2O_2 released by breast cancer cell line

Human breast cancer cells (MCF-7, MDA-MB-231 and T47D) obtained from the American Type Culture Collection (ATCC, Manassas, VA, USA). MCF-7, MDA-MB-231 and T47D were subsequently cultured on 10 cm^2 plates containing RPMI 1640 medium supplemented with 10% (*v*/v) heat inactivated fetal bovine serum, penicillin (100 k-units L^{-1}) and streptomycin (0.1 mg mL^{-1}) in a humidified incubator at 37 °C containing 5% CO_2. After sub-culture to 80–90% confluence, the cells were washed three time and collected by centrifuging. For electrochemical measurements, the amperometric current response to H_2O_2 released by approximately 5.0×10^6 cells was measured by Au-Pd/rGO modified GCE at 0.1 V (*vs.* Ag/AgCl) in 2 mL of PBS (0.1 M, pH 7.4), AA was injected to stimulate H_2O_2 release by the cells and current responses recorded by chronoamperometry. For comparison, the AA was also injected into PBS without cells and with cells containing catalase (Scheme 1).

3. Results and discussion

3.1. Structural and compositional characterization of Au-Pd/rGO nanocomposites

Representative SEM and TEM images at different magnifications of the as-prepared nanocomposites are shown in Fig. 1A-D. The SEM images showed that the Au-Pd nanocubes are dispersed uniformly on the surface of the rGO, and the exfoliated and large surface of the rGO are more wrinkled, which could be due to the reduction of GO. The rGO sheets form a more wrinkled and crumpled structure than the GO (Supplementary Fig. S1). The TEM patterns of the Au-Pd/rGO nanoalloys are shown in Fig. 1B, C and D. As shown in the figures, most of the Au-Pd nanoalloys have a cubic structure of approximately 40–65 nm diameter. Furthermore, EDX mapping of Au-Pd/rGO, presented in the insert of Fig. 1D, show that the Au-Pd nanoalloy possess a hexahedral structure.

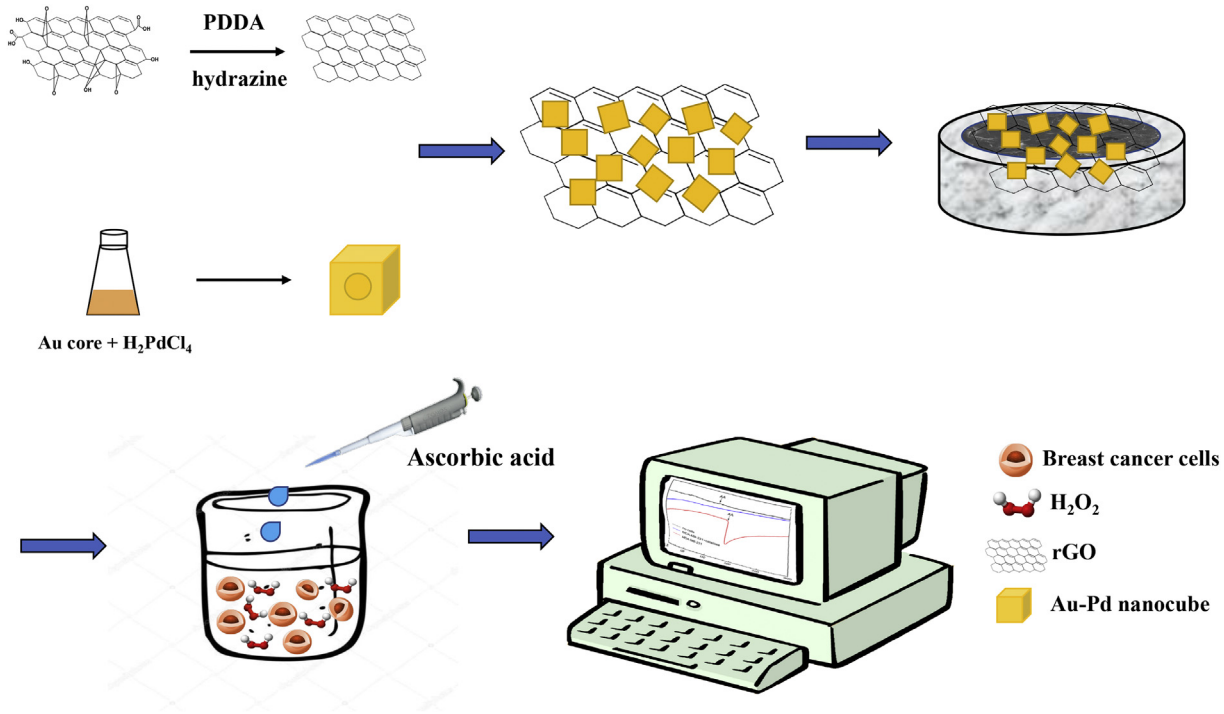

Scheme 1. Schematic illustration of the Au-Pd/rGO nanocube-modified GCE applied for the detection of H_2O_2 released from cells stimulated with ascorbic acid.

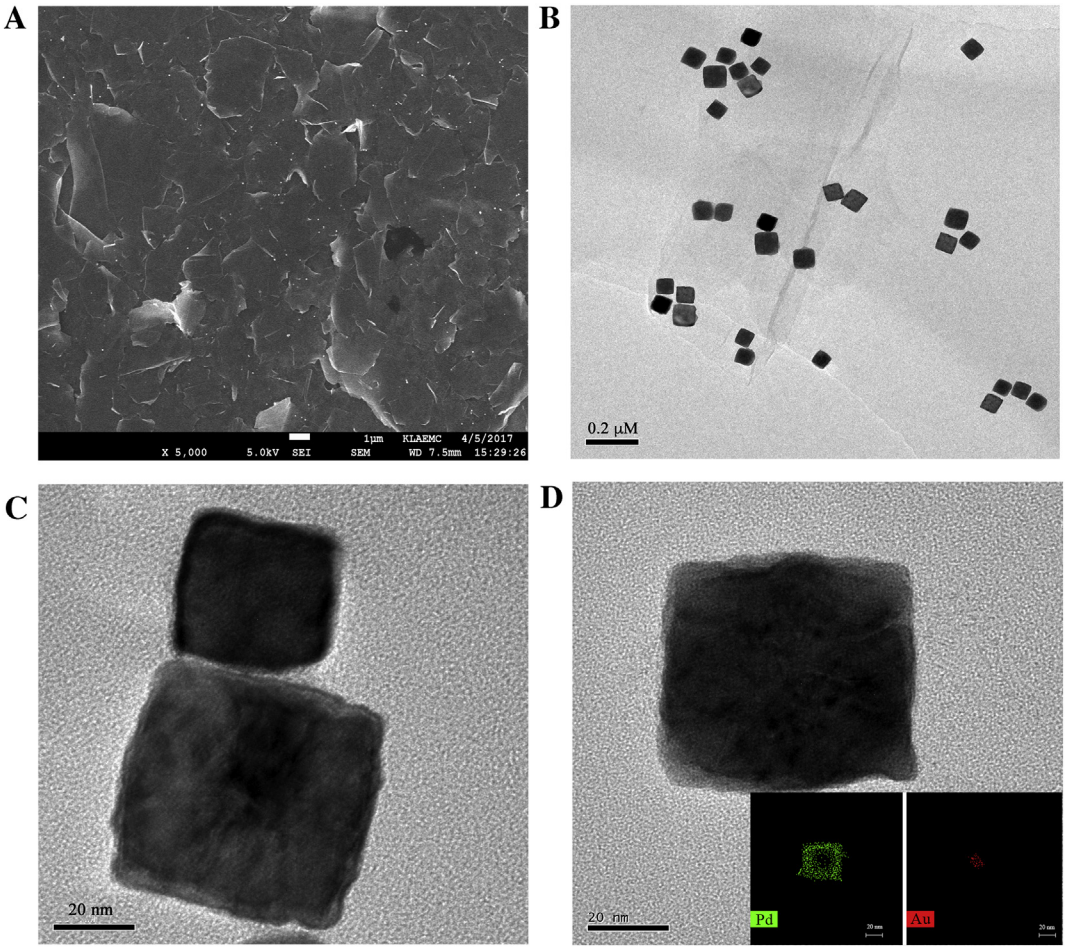

Fig. 1. (A) SEM patterns of Au-Pd/rGO nanocomposites. (B) and (C) TEM patterns of different magnifications of Au-Pd nanocubes. (D) TEM patterns of Au-Pd/rGO nanocomposites. The inset shows the elemental mapping image of a hexahedral Au-Pd nanoalloy.

EDX spectroscopy was employed to reveal the components of the final nanocomposites, which were rich in Pd and poor in Au (Fig. 2A), reflecting their nanoalloy structure. In addition, Fig. 2B demonstrates the XRD profiles of GO, rGO and Au-Pd/rGO, respectively. Both nanomaterials present a broad, weak peak at approximately 24° corresponding to graphitic planes [37]. For the XRD of Au-Pd/rGO, there are three strong diffraction peaks at approximately $2\theta = 39.95°$, 46.66° and 67.99° which can be assigned to the (111), (200) and (220) reflections of Au, and also peaks at $2\theta = 39.95°$, 46.66° and 67.99° corresponding to Pd (111), Pd (200) and Pd (220), suggesting that the Au-Pd nanoalloy has a face-centered cubic (FCC) structure and is fully crystalline in nature [23,27]. These results confirm the formation of the Au-Pd bimetallic nanocomposites.

3.2. Electrochemical sensing of H_2O_2 on Au-Pd/rGO nanocomposite-modified electrode

The as-prepared nanocomposites were used to modify electrodes separately in an electrochemical analyzer system. Before utilizing the proposed sensor for the electrochemical reduction of H_2O_2, a redox probe of ferricyanide ions was usually used to test the surface performance of bare GCE, rGO/GCE, Au-Pd/GCE and Au-Pd/rGO/GCE (Fig. 2C). Cyclic voltammetry (CV) was investigated in a 0.1 M KCl aqueous solution containing 10 mM $[Fe(CN)_6]^{3-}$. The interfacial properties of the electrode surface were evaluated based on the electroactive surface area, which was calculated by the Randles-Sevcik Eq. [38]:

$$I_p = 2.69 \times 10^5 \, AD^{1/2} ??^{3/2} \gamma^{1/2} C$$

where C is the concentration of the redox analyte (mol cm^{-3}); γ is the scan rate (mV/ s);?? represents the number of transition electrons in the redox processes whose value is equal to 1 for $[Fe(CN)_6]^{3-}$; D represents the diffusion coefficient of the molecule in solution, which is ($6.70 \pm 0.02 \times 10^{-6}$ cm^2 s^{-1}) for $K_3[Fe(CN)_6]$ [39]; A is the electroactive surface area (cm^2); and I_p is the peak current (A). Based on the Randles-Sevcik equation, the calculated electroactive surface area of Au-Pd/rGO/GCE was respectively 1.274, 1.517 and 1.875 times greater than the rGO/GCE, Au-Pd/GCE and bare GCE, suggesting that both Au-Pd nanocubes and the rGO nanocomposites can enhance the electroactive surface area due to their high-index facets and three-dimensional nanostructure. Consequently, we used Au-Pd/rGO/GCE to further study electrocatalytic activity to H_2O_2. Fig. 2D shows CV curves for Au-Pd/rGO/GCE in 0.1 M PBS (pH 7.4) in the presence and absence of H_2O_2 ranging from −0.6 V to 0.8 V. As depicted in Fig. 2D, an apparent reduction peak around 0.1 V was observed in the presence of 10 mM H_2O_2, indicating a relatively good response to the reduction of H_2O_2.

3.3. Optimization study of Au-Pd/rGO nanocomposites modified electrode to the reduction of H_2O_2

Our studies showed that the composite volume of the nanomaterial-modified electrode, the pH value and the scan rate have a great influence on the reduction sensitivity of H_2O_2. Fig. 3A shows that the sensitivity response enhanced with an increase in the volume of the Au-Pd/rGO nanocomposites used on electrodes, and reached a maximum at 6 μL; subsequently, response declined upon the addition of a larger volume of Au-Pd/rGO. The deposition of Au-Pd/rGO nanocomposites on

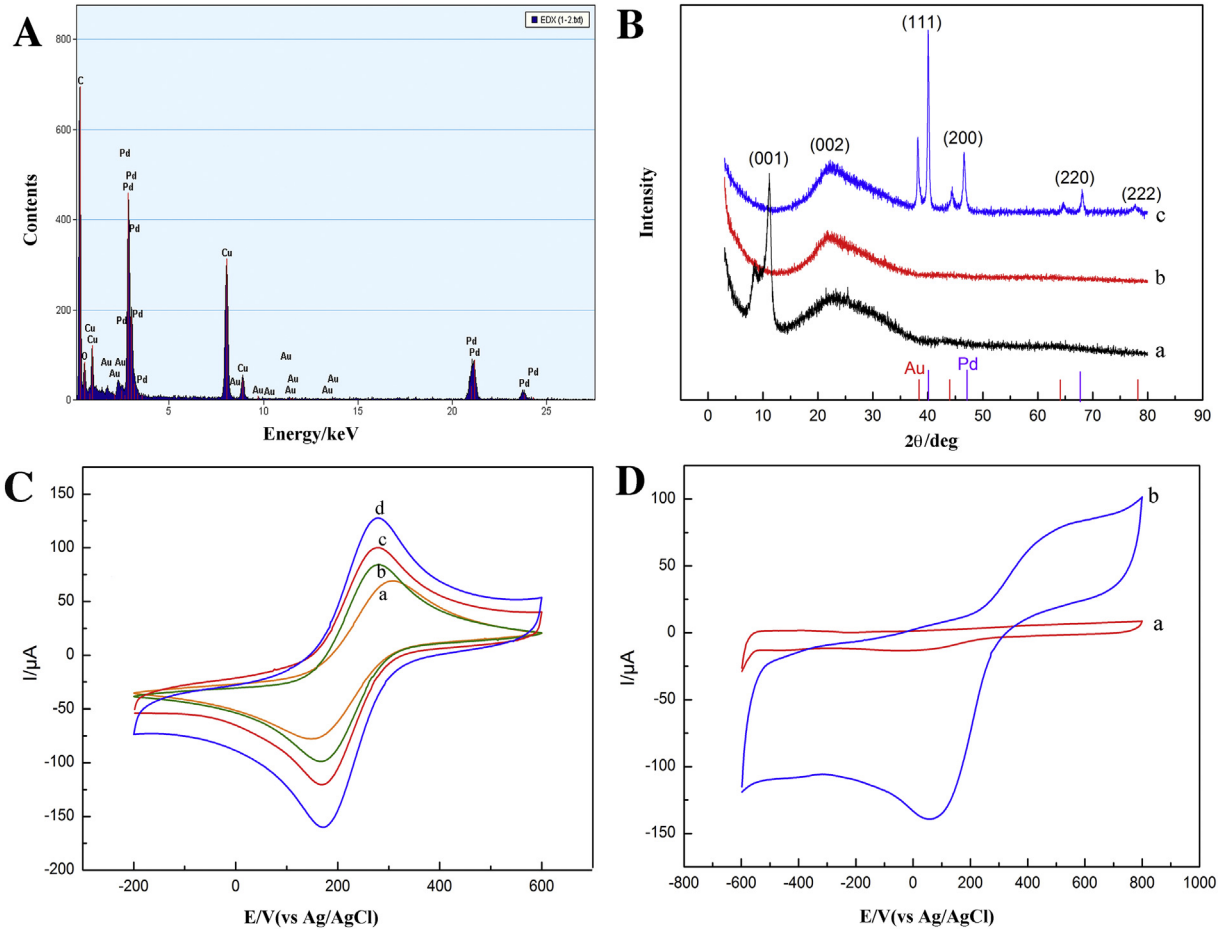

Fig. 2. (A) EDX patterns of Au-Pd/rGO nanocomposites. (B) XRD patterns of GO (a), rGO (b) and Au-Pd/rGO nanocomposites (c). (C) CVs of bare GCE (a), Au-Pd/GCE (b), rGO/GCE (c) and Au-Pd/rGO/GCE (d) recorded in a 0.1 M KCl solution containing 10 mM $[Fe(CN)_6]^{3-}$ at a scan rate of 50 mV/ s. (D) CVs of Au-Pd/rGO/GCE in 0.1 M PBS (pH 7.4) in the absence (a) and presence of 10 mM H_2O_2 (b) at a scan rate of 50 mV/ s.

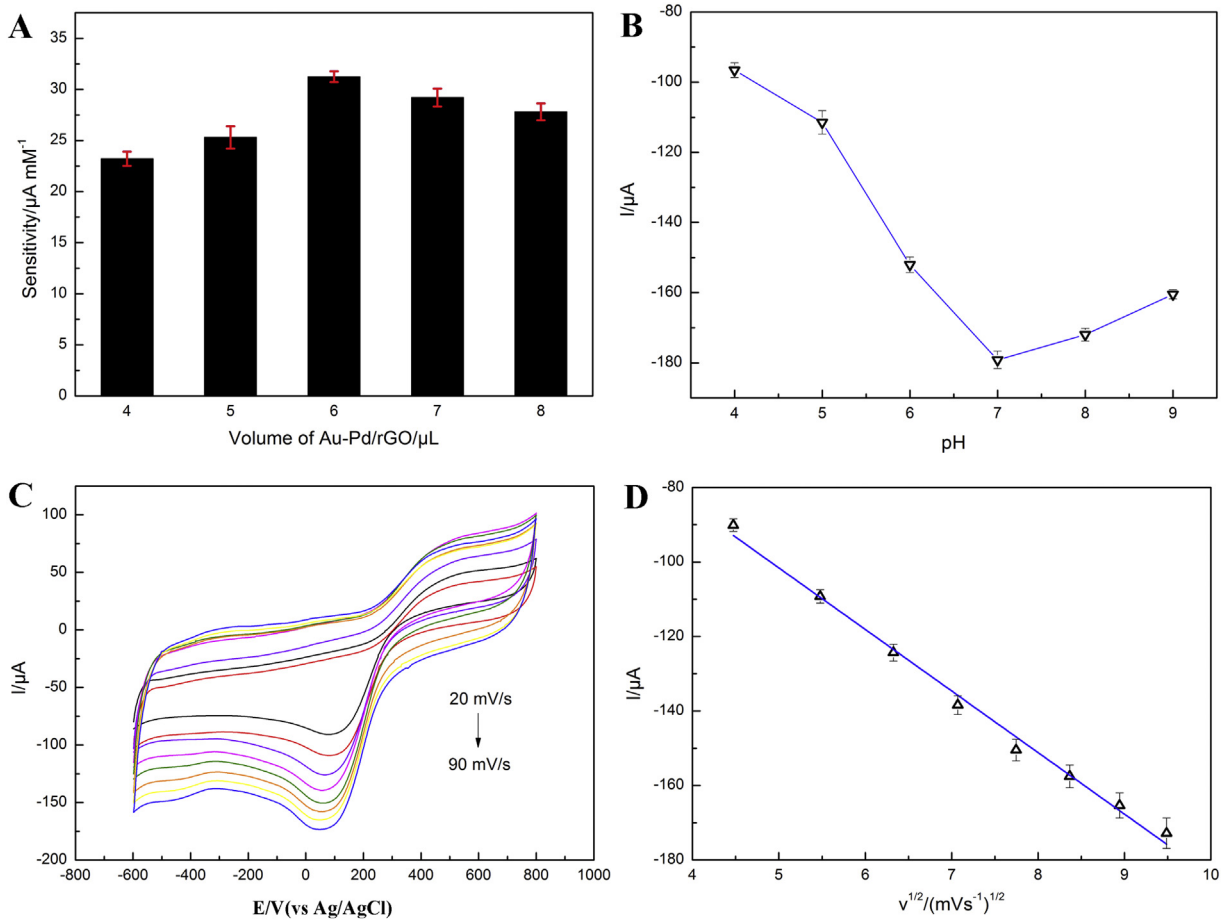

Fig. 3. (A) Optimization study of Au-Pd/rGO volume-modified GCE. (B) The effect of pH on the reduction peak current of 5 mM H_2O_2 in a 0.1 M PBS at a scan rate of 50 mV/s. (C) CVs of 5 mM H_2O_2 at Au-Pd/rGO/GCE with different scan rates in 0.1 M PBS (pH 7.4). Curves are obtained at 20,30,40,50,60,70,80 and 90 mV/ s, respectively. (D) The plot of the cathodic peak current *vs.* $v^{1/2}$.

the electrode thus required optimization because a high deposition could lead to high aggregation and low catalysis, while a low deposition led to low coverage and poor catalytic efficiency. The electrocatalytic reduction of H_2O_2 by Au-Pd/rGO nanocomposites in PBS at pH in the range 4.0 to 9.0 was also investigated (Fig. 3B). The reduction current reached a summit at pH 7, and thus a buffer solution at pH 7 was selected in subsequent experiments.

H_2O_2 reaction characteristics on Au-Pd/rGO/GCE and the Au-Pd/rGO nanocomposite films were studied by CV at scan rates ranging from 20 mV/s to 90 mV/s *vs.* Ag/AgCl (Fig. 3C). As the scan rate increased from 20 mV/s to 90 mV/s, the potential of the reduction peak increased and tended to a more negative direction. The cathodic peaks partially overlapped each other and widened with higher scan rate. Fig. 3D shows that the square root of the scan rate ($v^{1/2}$) was directly proportional to the anodic peak current (I_p), consistent with the model of Andrieux and Saveant [40], suggesting that the redox process on the Au-Pd/rGO-modified GCE surface is a quasi-reversible electrochemical process with fast electron transfer kinetics.

3.4. Amperometric response for H_2O_2 detection

Amperometric measurement was used to further study detection sensitivity of the as-prepared sensors. Fig. 4A shows the amperometric response of the rGO/GCE, Au-Pd/GCE and Au-Pd/rGO/GCE to successive injections with different concentrations of H_2O_2 in 0.1 M PBS (pH 7.4) at an operational potential of 0.1 *vs.* Ag/AgCl. As shown in Fig. 4A, the Au-Pd/rGO-modified electrode presented an enhanced amperometric response to H_2O_2, and moreover, upon each addition of H_2O_2, the steady-state current (≥ 95%) was reached within 4 s. However, a relatively low response and no clear response was observed on Au-Pd-modified and the rGO-modified GCE. Corresponding calibration curves are shown in Fig. 4B. The results show that the sensor has a linear relationship between H_2O_2 concentration and current, with the Au-Pd/rGO-modified GCE exhibiting a linear range from 0.005 μM to 1.0 mM (R^2 = 0.998) with a high sensitivity of 259.6 mA M^{-1} cm^{-2} based on n = 5 electrodes. The corresponding linear regression equation is I (μA) = −265.2C - 18.36. Alternatively, the linear relationship for the Au-Pd sensor is I (μA) = −46.1C - 8.95, with a sensitivity of 127 mA M^{-1} cm^{-2} based on n = 5 electrodes. As shown in Fig. 4C and D, the relevant linear ranges for the determination of H_2O_2 at the applied potential of 0.1 V comprised two sections: 0.005 μM to 1 mM and 1.0 mM to 3.5 mM, with correlation coefficient R^2 values of 0.998 and 0.997, respectively. The reason for two linear regions was probably a different H_2O_2 absorption and activation behavior on the Au-Pd/rGO catalyst under the different H_2O_2 concentrations [41]. Furthermore, the detection limit at a signal-to-noise factor ratio of 3 (S/N = 3) for the proposed sensor was estimated to be ~0.004 μM. Linear ranges, detection limits and measurement potentials for other reported H_2O_2 sensors are summarized in Table 1. These results suggest that the Au-Pd/rGO sensor possessed excellent electrocatalytic activity toward the reduction of H_2O_2 and could be a potential electrochemical sensor for high sensitively and for possible detection of H_2O_2 released from breast cancer cell lines.

A major barrier exists in using the proposed sensor for practical applications; the poor interference rejection ability of "universal" catalytic nanomaterials such as Au, Pt or Pd [25,42]. To investigate the selectivity of the Au-Pd/rGO sensor, chronoamperometry was undertaken in 0.1 M

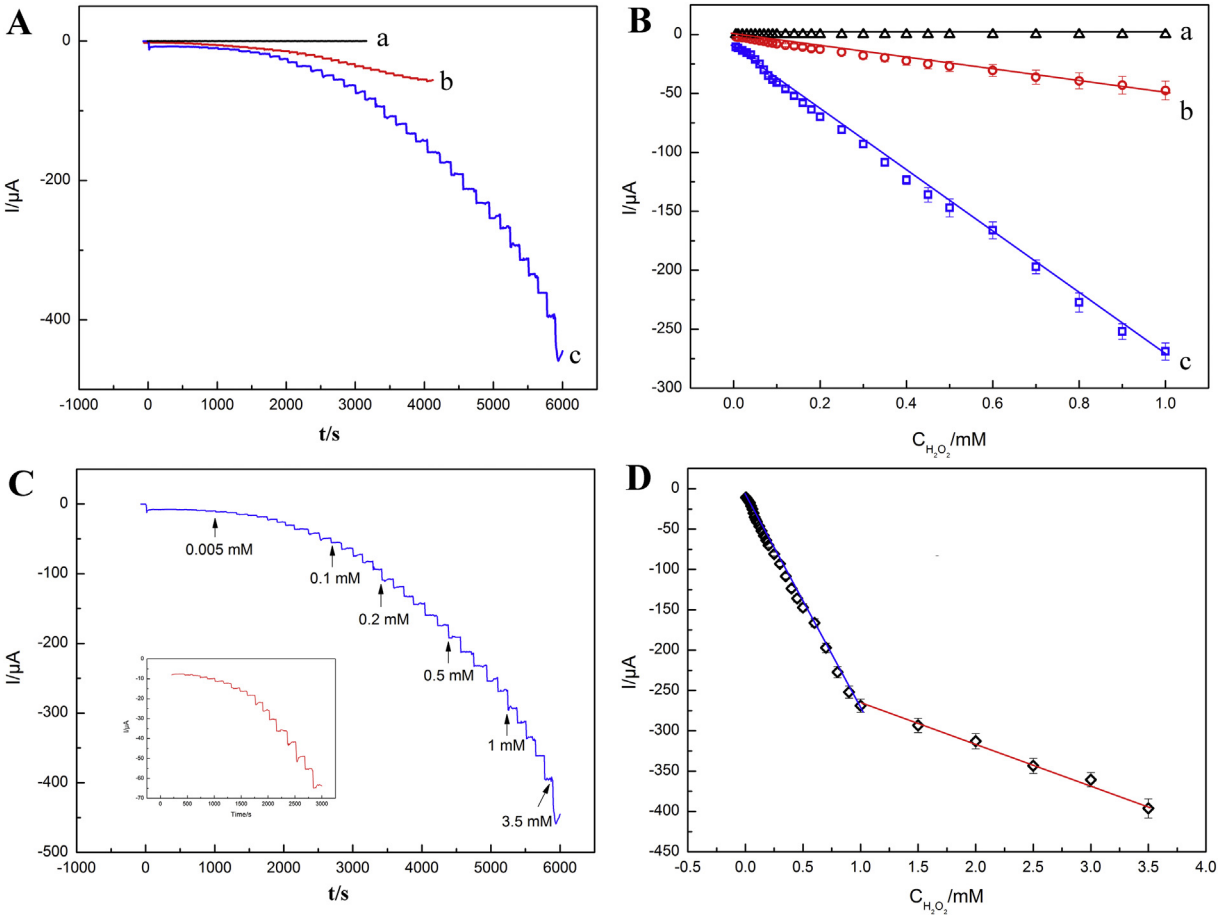

Fig. 4. (A) Amperometric i-t curves of rGO/GCE (a), Au-Pd/GCE (b) and Au-Pd/rGO/GCE (c) upon the successive addition of H_2O_2 to 0.1 M PBS (pH 7.4) under stirring. (B) Calibration curves of the response current *vs.* the H_2O_2 concentration for rGO/GCE (a), Au-Pd/GCE (b) and Au-Pd/rGO/GCE (c). (C) Amperometric i-t curves of Au-Pd/rGO/GCE in 0.1 M PBS (pH 7.4) with successive additions of H_2O_2. The inset shows a close look of the red oval region with an H_2O_2 concentration ranging from 0.005 μM to 0.1 mM. (D) The corresponding calibration curve of the response current *vs.* the concentrations of H_2O_2. (The corresponding linear equations are I (μA) = −265.2C - 18.36 (R^2 = 0.997) and I (μA) = −49.65C - 217.46 (R^2 = 0.998)).

PBS (pH 7.4) at a potential of 0.1 V. As shown in Supplementary Fig. S2, by addition of 0.1 mM H_2O_2, 1 mM AA, 1 mM UA, 1 mM AP, 1 mM GLU and 0.1 mM H_2O_2 showed no obvious current change observed in the presence of AA, UA, AP and GLU. This good selectivity of the sensor was attributed to the selection of an appropriate applied potential and nanocomposite fabrication.

In addition, good reproducibility and storage stability are significant for the evaluation of the performance of the H_2O_2 sensor. Good reproducibility with relative standard deviation (RSD) <2.9% was found for the proposed sensor according to a study of six independent electrodes. 86%–90.2% of its initial current response for H_2O_2 remained after one month. These results confirmed the acceptable reproducibility and reliability for the storage stability of the proposed sensor.

3.5. Application in real samples

To demonstrate the practical capability of the proposed sensor, a standard addition assay was used for the detection of H_2O_2 in human serum samples, which were diluted 60 times with 0.1 M PBS (pH 7.0); the results are listed in Table S2. The recovery ranged from 97.0% to 103.0%, and the relative standard deviation (RSD) was in a range 2.62% - 3.27%, which showed acceptable accuracy. To summarize, the proposed sensor has the capacity to detect H_2O_2 in physiological samples.

Table 1
Comparison of the reported electrodes for H_2O_2 determination.

Electrode materials	Detection potential (V)	Linear range (μM)	Detection limit (μM)	Ref
AuNFs/IL-GF paper	−0.6 (*vs* Ag/AgCl)	0.5–2300	0.1	[4]
CF@NCNTAs-GNPs	−0.3 (*vs* Ag/AgCl)	0.1–4300	0.05	[5]
HRP-MIL-100(Cr)-B	−0.3 (*vs* SCE)	0.5–3000	0.1	[15]
PtPd-Fe_3O_4/C	−0.25 (*vs* Ag/AgCl)	0.02–67	0.005	[41]
Mn_2O_3/Nf	0.65 (*vs* SCE)	0.1–1276.5	0.07	[48]
GQDs-CS/MB	−0.6 (*vs* SCE)	0.1–11,780	0.7	[49]
PtNPs-CDs/IL-GO	−0.08 (*vs* Ag/AgCl)	1–900	0.1	[50]
PtW/MoS_2	−0.25 (*vs* SCE)	1–200	0.005	[51]
Pd@Co_3O_4	0.6 (*vs* SCE)	0.01–3300	0.1	[52]
Au-Pd/rGO	0.1 (*vs* Ag/AgCl)	0.005–3500	0.004	This work

3.6. Detection of H_2O_2 released from living cells

Nowadays, reliable and accurate early prognostic methods for breast cancer are of great significance to the healthcare in women all over the world [43]. MCF-7, MDA-MB-231 and T47D cells are a common source of malignancies, and an important way to reduce risk is to realize a sensitive and effective detection method for cancer biomarkers at an early stage. Therefore, in this work, MCF-7, MDA-MB-231 and T47D were chosen as the model breast cancer cells, and AA used as the stimulant agent to trigger H_2O_2 generation [44,45]. Bright-field microscope images of the MCF-7, MDA-MB-231 and T47D cells are presented in Fig. 5A to C. Prior to electrochemical measurements, any toxic influence of the modified nanomaterials was studied by typical MTT assay (3-(4,5-dimethylthizaol-2-yl)-2,5-diphenyltetrazolium bromide) (Fig. 6). The results show that the living cancer cells had good cell viability of >90% after incubation with Au-Pd/rGO (2 μg mL^{-1}) for 24 h, indicating a good biocompatibility and electrode suitability for further measurements of H_2O_2 generated by living cells.

After verifying the biocompatibility of the prepared nanocomposites, we used these as a platform to monitor the H_2O_2 released from breast cancer cells (MCF-7, MDA-MB-231 and T47D). These cells are sensitive to many chemotactic stimulants [46]. Ascorbic acid (AA) is such a stimulant, and induces H_2O_2 generation in living cells with a more sustained chemotactic response. Also, as a result of stimulation by AA, respiratory burst occurs with H_2O_2 as the end product. Thus, AA was selected as stimulant in this study [47]. Taking MDA-MB-231 as an example, an enhanced reduction current was obtained by the injection of 10 μL of AA (200 ng mL^{-1}) when MDA-MB-231 cells were suspended in 0.1 M PBS (pH 7.4). As a control, PBS buffer without cells was also investigated (Fig. 5E). In addition, to testify the current change caused by the reduction of H_2O_2 generated by the MDA-MB-231 cells, catalase (300 U/mL) was added to the PBS buffer. As shown in Fig. 5E, there was no detectable current following the addition of catalase or in PBS without MDA-MB-231 cells. Meanwhile, under the same conditions, current changes were observed for MCF-7 and T47D; a comparison is presented in Fig. 5D and F. The absence of a current response will have resulted from catalase decomposition of released H_2O_2. Significantly, the amount of H_2O_2 released from the cells can be calculated from the standard curve. The recorded current changed by about 1.2 μA for MDA-MB-231, 1.17 μA for T47D and 0.56 μA for MCF-7, corresponding to 73.8 nM, 73.6 nM and 71.3 nM H_2O_2 generated from the cells (5.0×10^6 cells), respectively. These results further confirmed that the proposed sensor based on Au-Pd/rGO could be used to monitor the H_2O_2 released from cancer cells, and its potential applications can be explored for the early diagnosis of cancer.

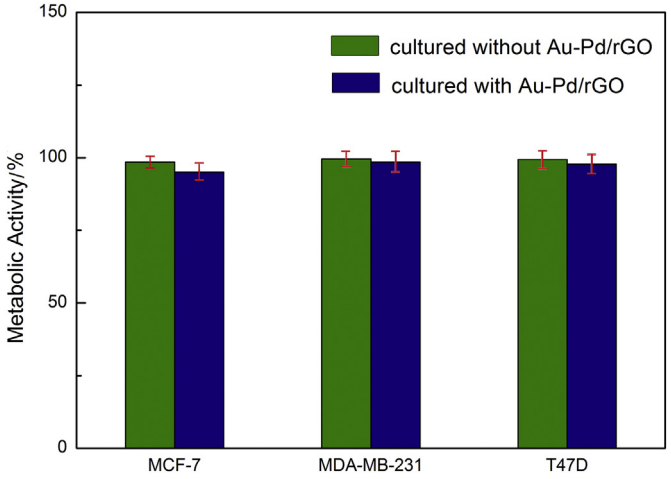

Fig. 6. Effects of the prepared Au-Pd/rGO/GCE on the metabolic activities of MCF-7, MDA-MB-231 and T47D cells.

4. Conclusions

We developed a high-performance sensor by taking advantage of the excellent electrocatalytic and high-index facets of Au-Pd nanocubes and the large surface area of rGO. The proposed sensor presented excellent electrocatalytic performance for the reduction of H_2O_2, which was attributed to the three-dimensional nanostructure used to modify the

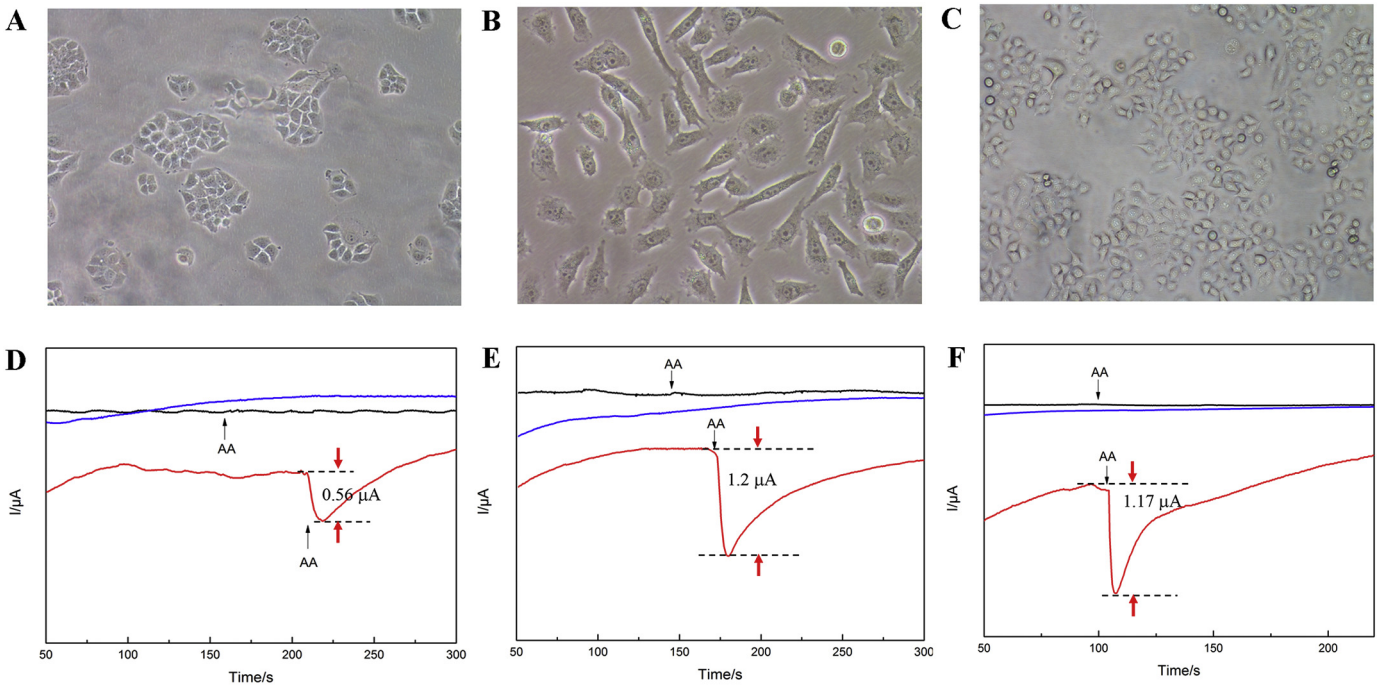

Fig. 5. The microscope images of MCF-7 (A), MDA-MB-231 (B) and T47D (C). Amperometric response of Au-Pd/rGO/GCE to injection of 10 μL AA (200 ng mL^{-1}) with and without MCF-7 (D), MDA-MB-231 (E) and T47D (F) cells in 0.1 M PBS (pH 7.4). (Black curve: no cells; blue curve: cells and catalase; red curve: cells only).

electrode surface and the enriched active sites. In consideration of this, Au-Pd/rGO nanocubes were used to fabricate a nano-enzymatic H_2O_2 sensor. Moreover, the sensor exhibited a wide linear range (0.005 μM to 3.5 mM), a low detection limit (4 nM), acceptable reproducibility and reliable storage stability. More significantly, the practical application of the biosensor was explored for the detection of endogenous H_2O_2 in human serum samples and for the real-time detection of H_2O_2 released from breast cancer cells, which further confirmed that the sensitive sensor can be used as a possible physiological and pathological H_2O_2 biosensor and is a possible valuable contribution to the early diagnosis of different cancers.

Acknowledgments

We are grateful to all laboratory members for their technical advice and helpful discussion. This work was supported by the National Natural Science Foundation of China (Grant No. 81671779) and the Key Projects of Tianjin Science and Technology Support Program (No. 16YFZCSY00440). The funders had no role in the study design, data collection and analysis, decision to publish, or preparation of the manuscript.

Appendix A. Supplementary data

Supplementary data to this article can be found online at https://doi.org/10.1016/j.bioelechem.2019.04.018.

References

[1] G.A. Colditz, K. Bohlke, Priorities for the primary prevention of breast cancer, CA Cancer J. Clin. 64 (2014) 186–194.
[2] American Cancer Society, Cancer Facts & Figures 2017, American Cancer Society, Atlanta, 2017.
[3] S. Mittal, H. Kaur, N. Gautam, A.K. Mantha, Biosensors for breast cancer diagnosis: a review of bioreceptors, biotransducers and signal amplification strategies, Biosens. Bioelectron. 88 (2017) 217–231.
[4] Y. Zhang, J. Xiao, Q. Lv, L. Wang, X. Dong, M. Asif, et al., In situ electrochemical sensing and real-time monitoring live cells based on freestanding nanohybrid paper electrode assembled from 3D functionalized graphene framework, ACS Appl. Mater. Interfaces 9 (2017) 38201–38210.
[5] Y. Zhang, J. Xiao, Y. Sun, L. Wang, X. Dong, J. Ren, et al., Flexible nanohybrid microelectrode based on carbon fiber wrapped by gold nanoparticles decorated nitrogen doped carbon nanotube arrays: in situ electrochemical detection in live cancer cells, Biosens. Bioelectron. 100 (2018) 453–461.
[6] Y.-E. Choi, J.-W. Kwak, J.W. Park, Nanotechnology for early cancer detection, Sensors 10 (2010).
[7] L. Wang, Q. Xiong, F. Xiao, H. Duan, 2D nanomaterials based electrochemical biosensors for cancer diagnosis, Biosens. Bioelectron. 89 (2017) 136–151.
[8] V. Jayanthi, A.B. Das, U. Saxena, Recent advances in biosensor development for the detection of cancer biomarkers, Biosens. Bioelectron. 91 (2017) 15–23.
[9] R. Abolhasan, A. Mehdizadeh, M.R. Rashidi, L. Aghebati-Maleki, M. Yousefi, Application of hairpin DNA-based biosensors with various signal amplification strategies in clinical diagnosis, Biosens. Bioelectron. 129 (2019) 164–174.
[10] D. Trachootham, J. Alexandre, P. Huang, Targeting cancer cells by ROS-mediated mechanisms: a radical therapeutic approach? Nat. Rev. Drug Discov. 8 (2009) 579–591.
[11] J. Alexandre, F. Batteux, C. Nicco, C. Chereau, A. Laurent, L. Guillevin, et al., Accumulation of hydrogen peroxide is an early and crucial step for paclitaxel-induced cancer cell death both in vitro and in vivo, Int. J. Cancer 119 (2006) 41–48.
[12] Z. Li, Y. Xin, Z. Zhang, New photocathodic analysis platform with quasi-core/shell-structured TiO_2@Cu_2O for sensitive detection of H_2O_2 release from living cells, Anal. Chem. 87 (2015) 10491–10497.
[13] C. Gao, Y. Tian, R. Zhang, J. Jing, X. Zhang, Endoplasmic reticulum-directed Ratiometric fluorescent probe for quantitive detection of basal H_2O_2, Anal. Chem. 89 (2017) 12945–12950.
[14] F. Liu, T. Bing, D. Shangguan, M. Zhao, N. Shao, Ratiometric fluorescent biosensing of hydrogen peroxide and hydroxyl radical in living cells with lysozyme-silver Nanoclusters: lysozyme as stabilizing ligand and fluorescence signal unit, Anal. Chem. 88 (2016) 10631–10638.
[15] H. Dai, W. Lu, X. Zuo, Q. Zhu, C. Pan, X. Niu, et al., A novel biosensor based on boronic acid functionalized metal-organic frameworks for the determination of hydrogen peroxide released from living cells, Biosens. Bioelectron. 95 (2017) 131–137.
[16] Z. Bai, G. Li, J. Liang, J. Su, Y. Zhang, H. Chen, et al., Non-enzymatic electrochemical biosensor based on Pt NPs/RGO-CS-fc nano-hybrids for the detection of hydrogen peroxide in living cells, Biosens. Bioelectron. 82 (2016) 185–194.
[17] B. Ma, C. Kong, X. Hu, K. Liu, Q. Huang, J. Lv, et al., A sensitive electrochemical non-enzymatic biosensor for the detection of H_2O_2 released from living cells based on ultrathin concave Ag nanosheets, Biosens. Bioelectron. 106 (2018) 29–36.
[18] Z. Li, Y. Xin, W. Wu, B. Fu, Z. Zhang, Topotactic conversion of copper(I) phosphide nanowires for sensitive electrochemical detection of H_2O_2 release from living cells, Anal. Chem. 88 (2016) 7724–7729.
[19] N. Wang, Y. Han, Y. Xu, C. Gao, X. Cao, Detection of H_2O_2 at the nanomolar level by electrode modified with ultrathin AuCu nanowires, Anal. Chem. 87 (2015) 457–463.
[20] Y.K. Kho, A. Iwase, W.Y. Teoh, L. Mädler, A. Kudo, R. Amal, Photocatalytic H2 evolution over TiO_2 nanoparticles. The synergistic effect of Anatase and rutile, J. Phys. Chem. C 114 (2010) 2821–2829.
[21] B. Wu, S. Hou, Y. Xue, Z. Chen, Electrodeposition(−) assisted assembled multilayer films of gold nanoparticles and glucose oxidase onto Polypyrrole-reduced Graphene oxide matrix and their Electrocatalytic activity toward glucose, Nanomaterials (Basel) 8 (2018) 993.
[22] S. Zhang, R. Li, X. Liu, L. Yang, Q. Lu, M. Liu, et al., A novel multiple signal amplifying immunosensor based on the strategy of in situ-produced electroactive substance by ALP and carbon-based Ag-au bimetallic as the catalyst and signal enhancer, Biosens. Bioelectron. 92 (2017) 457–464.
[23] R. Li, T. Yang, Z. Li, Z. Gu, G. Wang, J. Liu, Synthesis of palladium@gold nanoalloys/nitrogen and sulphur-functionalized multiple graphene aerogel for electrochemical detection of dopamine, Anal. Chim. Acta 954 (2017) 43–51.
[24] J. Feng, Y. Li, M. Li, F. Li, J. Han, Y. Dong, et al., A novel sandwich-type electrochemical immunosensor for PSA detection based on PtCu bimetallic hybrid (2D/2D) rGO/g-C3N4, Biosens. Bioelectron. 91 (2017) 441–448.
[25] Y. Sun, M. Luo, X. Meng, J. Xiang, L. Wang, Q. Ren, et al., Graphene/intermetallic PtPb Nanoplates composites for boosting electrochemical detection of H2O2 released from cells, Anal. Chem. 89 (2017) 3761–3767.
[26] W. Dong, Y. Ren, Z. Bai, J. Jiao, Y. Chen, B. Han, et al., Synthesis of tetrahexahedral Au-Pd core–shell nanocrystals and reduction of graphene oxide for the electrochemical detection of epinephrine, J. Colloid Interf. Sci. 512 (2018) 812–818.
[27] C.-L. Lu, K.S. Prasad, H.-L. Wu, J.-a.A. Ho, M.H. Huang, Au Nanocube-directed fabrication of Au—Pd Core—Shell Nanocrystals with Tetrahexahedral, concave octahedral, and octahedral structures and their Electrocatalytic activity, J. Am. Chem. Soc. 132 (2010) 14546–14553.
[28] G. Somorjai, Chemistry in Two Dimensions: Surfaces, Cornell U, Press, Ithaca, 1981 479.
[29] N. Tian, Z.-Y. Zhou, S.-G. Sun, Y. Ding, Z.L. Wang, Synthesis of tetrahexahedral platinum nanocrystals with high-index facets and high electro-oxidation activity, science 316 (2007) 732–735.
[30] N. Kakati, J. Maiti, K.S. Lee, B. Viswanathan, Y.S. Yoon, Hollow sodium nickel fluoride nanocubes deposited MWCNT as an efficient Electrocatalyst for urea oxidation, Electrochim. Acta 240 (2017) 175–185.
[31] S. Park, R.S. Ruoff, Chemical methods for the production of graphenes, Nat. Nanotechnol. 4 (2009) 217–224.
[32] D. Luo, G. Zhang, J. Liu, X. Sun, Evaluation criteria for reduced graphene oxide, J. Phys. Chem. C 115 (2011) 11327–11335.
[33] T. Yoon, J.H. Kim, J.H. Choi, D.Y. Jung, I.J. Park, S.Y. Choi, et al., Healing graphene defects using selective electrochemical deposition: toward flexible and stretchable devices, ACS Nano 10 (2016) 1539–1545.
[34] G. Darabdhara, B. Sharma, M.R. Das, R. Boukherroub, S. Szunerits, Cu-Ag bimetallic nanoparticles on reduced graphene oxide nanosheets as peroxidase mimic for glucose and ascorbic acid detection, Sensors Actuat. B Chem. 238 (2017) 842–851.
[35] X. Li, X. Du, Molybdenum disulfide nanosheets supported Au-Pd bimetallic nanoparticles for non-enzymatic electrochemical sensing of hydrogen peroxide and glucose, Sensors Actuat. B Chem. 239 (2017) 536–543.
[36] W. Dong, Y. Ren, Y. Zhang, Y. Chen, C. Zhang, Z. Bai, et al., Synthesis of Pb nanowires-Au nanoparticles nanostructure decorated with reduced graphene oxide for electrochemical sensing, Talanta 165 (2017) 604–611.
[37] L. Tang, Y. Wang, Y. Li, H. Feng, J. Lu, J. Li, Preparation, structure, and electrochemical properties of reduced graphene sheet films, Adv. Funct. Mater. 19 (2009) 2782–2789.
[38] A.J. Bard, L.R. Faulkner, Electrochemical Methods : Fundamentals and Applications, John Wiley, 1980.
[39] M. Ma, T. Zhe, Y. Ma, Z. Wang, Q. Chen, J. Wang, Highly sensitive and reproducible non-enzymatic glucose sensor fabricated by drop-casting novel nanocomposite with 3D architecture and tailorable properties prepared in controllable way, Talanta 180 (2018) 133–143.
[40] C.P. Andrieux, J.M. Saveant, Heterogeneous (chemically modified electrodes, polymer electrodes) vs. homogeneous catalysis of electrochemical reactions, Electroanal. Chem. 93 (1978) 163–168.
[41] X. Sun, S. Guo, Y. Liu, S. Sun, Dumbbell-like PtPd–Fe3O4 nanoparticles for enhanced electrochemical detection of H_2O_2, Nano Lett. 12 (2012) 4859–4863.
[42] X.H. Niu, L.B. Shi, H.L. Zhao, M.B. Lan, Advanced strategies for improving the analytical performance of Pt-based nonenzymatic electrochemical glucose sensors: a minireview, Anal. Methods 8 (2016) 1755–1764.
[43] T. Zhang, Y. Gu, C. Li, X. Yan, N. Lu, H. Liu, et al., Fabrication of novel electrochemical biosensor based on Graphene Nanohybrid to detect H_2O_2 released from living cells with ultrahigh performance, ACS Appl. Mater. Interfaces 9 (2017) 37991–37999.
[44] H. Chang, X. Wang, K.K. Shiu, Y. Zhu, J. Wang, Q. Li, et al., Layer-by-layer assembly of graphene, Au and poly(toluidine blue O) films sensor for evaluation of oxidative stress of tumor cells elicited by hydrogen peroxide, Biosens. Bioelectron. 41 (2013) 789–794.
[45] Y. Zhang, X. Bai, X. Wang, K.-K. Shiu, Y. Zhu, H. Jiang, Highly sensitive graphene–Pt Nanocomposites Amperometric biosensor and its application in living cell H_2O_2 detection, Anal. Chem. 86 (2014) 9459–9465.

[46] A.W. Griffith, J.M. Cooper, Single-cell measurements of human neutrophil activation using electrorotation, Anal. Chem. 70 (1998) 2607–2612.
[47] P. Wu, Y. Qian, P. Du, H. Zhang, C. Cai, Facile synthesis of nitrogen-doped graphene for measuring the releasing process of hydrogen peroxide from living cells, J. Mater. Chem. 22 (2012) 6402–6412.
[48] C. Cheng, Y. Huang, N. Wang, T. Jiang, S. Hu, B. Zheng, et al., Facile fabrication of Mn_2O_3 nanoparticle-assembled hierarchical hollow spheres and their sensing for hydrogen peroxide, ACS Appl. Mater. Interfaces 7 (2015) 9526–9533.
[49] F. Mollarasouli, K. Asadpour-Zeynali, S. Campuzano, P. Yáñez-Sedeño, J.M. Pingarrón, Non-enzymatic hydrogen peroxide sensor based on graphene quantum dots-chitosan/methylene blue hybrid nanostructures, Electrochim. Acta 246 (2017) 303–314.
[50] D. Chen, X. Zhuang, J. Zhai, Y. Zheng, H. Lu, L. Chen, Preparation of highly sensitive Pt nanoparticles-carbon quantum dots/ionic liquid functionalized graphene oxide nanocomposites and application for H_2O_2 detection, Sensors Actuat. B Chem. 255 (2018) 1500–1506.
[51] L. Zhu, Y. Zhang, P. Xu, W. Wen, X. Li, J. Xu, PtW/MoS_2 hybrid nanocomposite for electrochemical sensing of H_2O_2 released from living cells, Biosens. Bioelectron. 80 (2016) 601–606.
[52] J. Xi, Y. Zhang, N. Wang, L. Wang, Z. Zhang, F. Xiao, et al., Ultrafine Pd nanoparticles encapsulated in microporous Co_3O_4 hollow Nanospheres for in situ molecular detection of living cells, ACS Appl. Mater. Interfaces 7 (2015) 5583–5590.